NANO LETTERS

2005
Vol. 5, No. 9
1726−1729

Focusing Surface Plasmons with a Plasmonic Lens

Zhaowei Liu,† Jennifer M. Steele,† Werayut Srituravanich, Yuri Pikus, Cheng Sun, and Xiang Zhang*

NSF Nanoscale Science and Engineering Center (NSEC), 5130 Etcheverry Hall, University of California, Berkeley, California 94720

Received May 31, 2005; Revised Manuscript Received June 28, 2005

ABSTRACT

We report the focusing of surface plasmon polaritons by circular and elliptical structures milled into optically thick metallic films or plasmonic lenses. Both theoretical and experimental data for the electromagnetic nearfield is presented. The nearfield is mapped experimentally using nearfield scanning optical microscopy and plasmonic lithography. We find that the intensity at the focal points of the plasmonic lenses increases with size.

Surface plasmon polariton (SPP) excitations on films and planar metallic structures allow for the manipulation of light on subwavelength scales, opening up possible applications such as sensing[1−5] and plasmonic optical devices.[4,6−9] Although the electromagnetic fields of SPPs decay exponentially normal to the surface, for noble metals, their propagation lengths along surfaces can reach tens of microns.[10] This has allowed the realization of two-dimensional plasmonic optical components such as mirrors,[11,12] waveguides,[9,13,14] and interferometers.[6,12] In this paper, we concentrate on circular and elliptical structures in metallic films, or plasmonic lenses, that excite as well as focus the electromagnetic energy of SPPs.

Previous studies on the focusing of SPPs have investigated using surface defects to reflect SPPs.[6,12,15,16] But because SPPs have a low reflection coefficient,[17,18] the amount of energy reflected is likely insufficient for many proposed applications.[16] One way to increase the SPP reflection from surface defects is to introduce periodic surface defects to increase the reflection through Bragg scattering.[6,12] In this work, we obtain focusing not by reflection but by directionally exciting the SPPs toward the focus points. Instead of surface defects, the sharp edge of a slit milled through a metallic film was used to couple light into SPPs. The edge can be thought of as a line of SPP point sources. If the slit width is smaller than half of the incident wavelength of light, no propagating modes are possible and a majority of the light is diffracted.[19−21] This diffracted light gains a Δk in the direction along the film, allowing a portion of the incident light to excite a SPP.[10,22] The wave vector of the SPP will be selected by the metallic surface according to its dispersion curve, and will therefore depend on the frequency of incident light and the dielectric functions of the metal and the surrounding media.[10] The direction of the wave vector, which determines the energy propagation direction, will be normal to the slit if the incident light is normal to the metal film. Consequentially, in the case of a plasmonic lens the energy will be guided toward the focal points of the lens. Because this is not a resonant process as in the case of a grating or particle, only a small fraction of the incident light will be coupled to the SPP. However, because a large band of k will be excited by the edge, different wavelengths of light may be used to excite surface plasmons on the same sample. This is an advantage over periodic surface defects, which will only efficiently reflect SPPs for a specified SPP wavelength.

The electromagnetic nearfield distribution resulting from focused SPPs was recorded in two ways: nearfield scanning microscopy (NSOM) and plasmonic lithography. In both cases, metallic films were first evaporated onto a quartz plate. Then patterns were milled through the film using an FEI Strata 201 XP focused ion beam (FIB). For the NSOM measurements, 514 nm light from a Spectra-Physics 2000 argon ion laser was incident on the quartz side of the sample, and the nearfield intensity was measured with a metal-plated NSOM tip on the opposite side, shown schematically in Figure 1a. Silver films were used in the NSOM experiments because of its long SPP propagation lengths in the visible region. The laser light was linearly polarized in the direction shown by the arrow in Figure 1c. Because of the polarization, only the portions of the circle where a component of the incident electric field was perpendicular to the circle edge will excite SPPs. For the plasmonic lithography experiments, the patterned metallic films were spin coated with a thin layer of photoresist, shown in Figure 1b. The sample was then

* Corresponding author. E-mail: xiang@berkeley.edu.
† The first two authors contributed equally to this work.

10.1021/nl051013j CCC: $30.25
Published on Web 07/29/2005

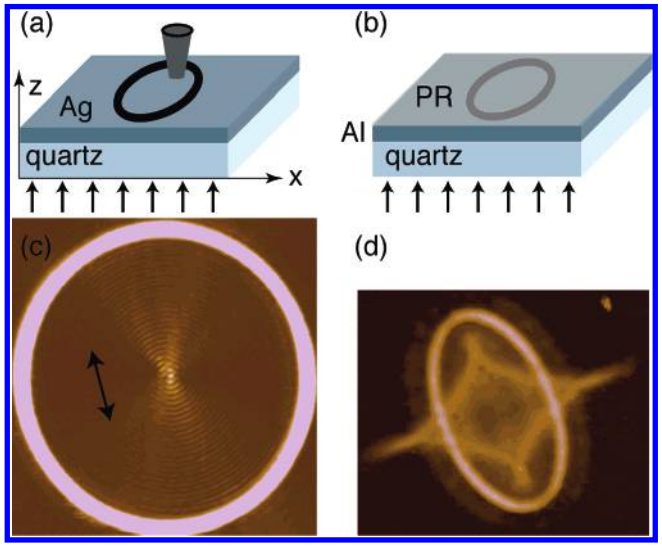

Figure 1. Experimental setup for (a) NSOM and (b) plasmonic lithography measurements for recording the nearfield pattern for plasmonic lenses. (c) Nearfield pattern for a 14 μm diameter circle cut into a 150 nm thick silver film recorded with NSOM. Polarization of incident light is indicated with an arrow. (d) Nearfield pattern for an ellipse with a long axis of approximately 4 μm and a short axis of 2.5 μm cut into a 70 nm thick aluminum film recorded with plasmonic lithography.

illuminated from the quartz side with the i-line (365 nm) of a mercury lamp. The lamp provides unpolarized light to excite the SPPs, allowing for the entire edge of the pattern to excite SPPs uniformly. For the plasmonic lithography experiments, aluminum was chosen because its SPP propagation lengths in the UV region are longer than those of silver. After exposure for a few seconds, the resist was chemically developed to record the nearfield patterns. This method is similar to the photochemical imaging outlined recently.[23]

The NSOM and plasmonic lithography methods measure different aspects of the electromagnetic nearfield of the SPPs. It is generally accepted that NSOM tips are more sensitive to the component of the electric field parallel to the surface, but this is still under debate.[24] However, the photoresist is sensitive to the total electromagnetic intensity and therefore measures the total electric field, both parallel and perpendicular to the surface. Although the plasmonic lithography method has an advantage over NSOM measurements in that it gives the full plasmonic response, the resist only records regions in which the local electromagnetic field intensity is above the exposure threshold for the photoresist and cannot distinguish different intensity levels above threshold. It is therefore difficult to resolve the fine details of nearfield patterns that contain a large range of intensities or poor contrast of high to low intensity areas. These two methods for recording the nearfield yield important information, and it is therefore instructive to consider them both.

Circles of different diameters were cut through a 150 nm thick silver film. The average slit width for all of the circles measured was 283 $\pm$ 23 nm. The surface roughness of the silver was measured with a Digital Instruments atomic force microscope (AFM) to be under 5 nm. The thickness of the silver film was chosen to be several times the skin depth, here 27 nm, to eliminate the direct transmission of light through the film. This ensures that all fringes measured are the result of SPP interference and not interference with directly transmitted light.[25] Figure 1c shows a representative nearfield pattern collected by NSOM for a 14 μm diameter circle. SPPs excited normal to the slits are focused into the center of the circle, interfering with each other to create a standing wave. The period of the interference fringes is therefore expected to be half of that of the SPP wavelength. For 514 nm light incident on silver, the SPP wavelength is 490 nm, giving an interference period of 245 nm. This agrees very well with the measured period of 244 nm. Also apparent in Figure 1c is that the intensity is highest at the center of the circle. Plasmonic lithography measurements of the circles cut into aluminum films only show a peak in the middle of the circle because of the large relative intensity at the focus point. Even with optimizing the exposure parameters, it was not possible to duplicate the detail obtained with NSOM.

Elliptically shaped slits were milled into 70 nm thick aluminum films. The skin depth for Al in the UV is approximately 13 nm, so the directly transmitted light is almost completely attenuated and the recorded nearfield pattern results solely from SPP excitations. Figure 1d shows the AFM profile of developed resist for an ellipse fabricated with a long axis of approximately 4 μm and a short axis of 2.5 μm. The SPPs are excited normally from the ellipse edge, and the pattern created is precisely what one would obtain if normal lines were drawn from the circumference of the ellipse. The two interior focal points of the ellipse are clearly visible. As the SPPs travel along the film and encounter the opposite side of the ellipse, portions of the SPP wave will either be reflected or transmitted. The two additional focal points visible outside the ellipse indicate that the SPPs launched on the film are transmitted mostly through the slits on the opposite side of the ellipse. This agrees with other similar experimental results that report high transmission of SPPs through slits in metallic films.[17,18,26] NSOM images of the ellipses did not reveal any additional information, and therefore are not included here.

The optical response of the circles was modeled using Microwave Studio (MWS), a computer program that calculates the electromagnetic response of metallic and dielectric objects using a method based on the finite difference time domain (FDTD) method. To minimize the computation size and time, we simulated a silver disk of the same height and diameter instead of a circle cut into a silver slab. The edge of the disk will diffract the light similar to the slits, but the coupling efficiency is likely to be different because of the difference in geometry. Figure 2a and b show the x and z components of the intensity of the electromagnetic field just above the silver surface, respectively. One notable difference is the intensity at the center of the circle. Charge conservation dictates that the x component of the electric field must reach a maximum at the center while the z component vanishes.[27] The calculations also show that the ratio of $|E_x|^2$ to $|E_z|^2$ is about 1:10.

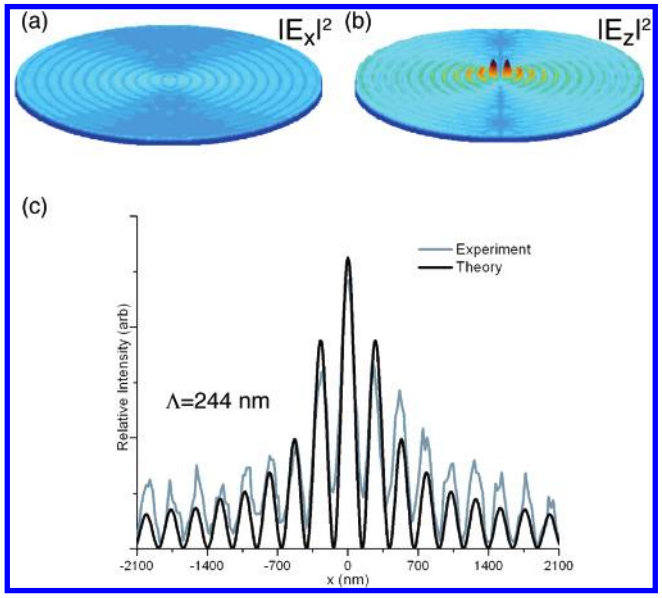

Figure 2. Calculated intensity for the x (a) and z (b) component of the electric field for a silver disk 150 nm thick with a diameter of 6 μm. (c) Comparison of the cross section of the calculated $|E_x|^2$ for the disk in a and the measured NSOM intensity for a circle milled into a 150 nm thick silver film with a 6 μm diameter. The period of the fringes is 244 nm.

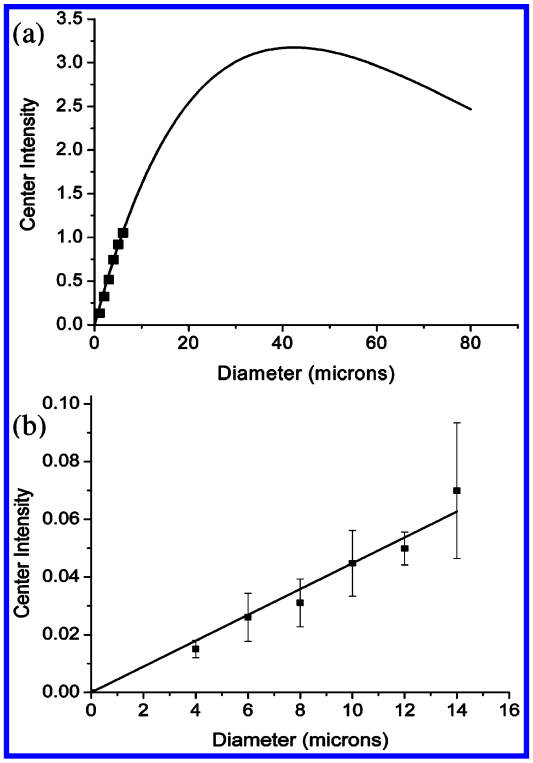

Figure 3. (a) Intensity at the center of the lens calculated using eq 1. Dots show $|E_x|^2$ calculated by MWS. (b) NSOM measurement of the intensity at the center of the circle normalized to the intensity measured in the slit as a function of diameter.

The experimental results show a maximum in the center of the circle indicating that the NSOM tip is more sensitive to E_x as predicted by theoretical studies[24] despite the larger contribution of E_z to the total intensity. To determine to what extent E_z contributes to the measured NSOM intensity, the cross section of the experimental data and the calculated cross section of $|E_x|^2$ was plotted together for a 6 μm diameter circle in Figure 2c. Very good agreement is achieved between simulation and experiment, validating the assertion that the NSOM tip preferentially measures $|E_x|^2$ and approximating the circle as a disk. Additionally, the measured period is half of the SPP wavelength, indicating that the interference pattern indeed consists of only interfering SPP waves on the silver-air side of the sample and contains no contributions from the incident light or SPPs excited on the silver-quartz side.[25]

Assuming that the edge of the slit acts like a line source of SPPs, the intensity at the center of the circle will be proportional to the circle circumference divided by the circumference of the area inside the circle of highest intensity. Therefore, as the diameter of the circle is increased, more energy will be coupled into the SPPs, and the intensity at the center will increase. Approximating the area in the center of the circle with the highest intensity as a circle with a diameter of one interference fringe, the circumference will be $\pi(\lambda_{sp}/2)$ where λ_{sp} is the wavelength of the SPP excited along the film. The intensity in the center will then be enhanced by a ratio of the milled circle circumference ($2\pi r$) to the inner circumference. However, as the radius of the milled circle approaches the propagation length of the SPPs, the enhancement will be reduced through loss as the SPPs are damped out. The expression for these two competing processes is therefore

$$I = CI_0 \frac{4r}{\lambda_{sp}} e^{(-(r/l_{sp}))} \quad (1)$$

where I_0 is the incident intensity, r is the radius of the circle, l_{sp} is the propagation length for the SPP, and C is the coupling efficiency of the slit. C is a complicated function of the slit geometry and will likely have a different functional form when the slit width is much larger or much smaller than the incident wavelength. Equation 1 is plotted along with $|E_x|^2$ at the center of the circle as a function of diameter as calculated by MWS in Figure 3a using the coupling efficiency as a fitting parameter. The dependence on the diameter of the circle is roughly linear for diameters much less than the SPP propagation length for silver at the incident wavelength, here 20.4 μm. Beyond the SPP propagation length, the intensity begins to decrease as the SPPs are damped out before reaching the center.

Figure 3b shows data measured experimentally using NSOM. The intensity in the center of the circle was normalized to the maximum intensity recorded in the slit region by the NSOM tip. Each point represents an average of several samples fabricated and measured under identical illumination conditions with the same NSOM tip. The line is a linear fit to the data, which is expected for the range of diameters accessible experimentally. In general, the error increases with the diameter of the circle. Because each point is an average of the same number of samples, the increase in error is likely due to the larger area of these circles. The longer the path the SPPs have to travel to reach the center, the more likely they are to encounter a surface defect, and the effect of the surface defects on the overall pattern will be greater.

Although the measured intensity in the circle is weak, because the NSOM tip preferentially measures $|E_x|^2$, the actual intensity is likely to be much larger because of the fact that the calculated ratio of $|E_x|^2$ to $|E_z|^2$ using MWS is about 1:10. From eq 1, in the region where the radius is much less than the surface plasmon propagation length, the center intensity is linear in r and the coupling efficiency may be calculated from the slope. For the specific geometry measured here, the coupling efficiency extracted was 0.1%, which is in the range of other reported efficiencies for similar geometries.[28] However, the actual coupling efficiency is likely to be higher again due to the NSOM tip preferentially measuring $|E_x|^2$.

In conclusion, we have demonstrated that circular and elliptical slit structures on metal film can act as plasmonic lenses that can focus surface plasmons. Excited by either circular or elliptical slits, the propagating SPP waves interfere, concentrating the electromagnetic field at the focal points. For circles, as the diameter of the circle is increased, the intensity at the center of the circle also increases. Because plasmonic lenses can manipulate electromagnetic waves on subwavelength scales, they can be utilized as fundamental tools in nanooptics[6−9] as well as in applications such as sensing[4] and optoelectronic devices.[8,11,13]

Acknowledgment. This work is supported by the Center for Scalable and Integrated Nanomanufacturing (SINAM), the NSF Nanoscale Science and Engineering Center (NSEC) under award number DMI-0327077, and an NSF grant DMI-0218273.

References

(1) Dahlin, A.; Zach, M.; Rindzevicius, T.; Kall, M.; Sutherland, D. S.; Hook, F. *J. Am. Chem. Soc.* **2005**, *127*, 5043−5048.
(2) Haes, A. J.; Van Duyne, R. P. *Anal. Bioanal. Chem.* **2004**, *379*, 920−930.
(3) Haes, A. J.; Zou, S. L.; Schatz, G. C.; Van Duyne, R. P. *J. Phys. Chem. B* **2004**, *108*, 6961−6968.
(4) Hutter, E.; Fendler, J. H. *Adv. Mater.* **2004**, *16*, 1685−1706.
(5) Van Duyne, R. P. *Science* **2004**, *306*, 985−986.
(6) Drezet, A.; Stepanov, A. L.; Ditlbacher, H.; Hohenau, A.; Steinberger, B.; Aussenegg, F. R.; Leitner, A.; Krenn, J. R. *Appl. Phys. Lett.* **2005**, *86*, 074104.
(7) Salerno, M.; Krenn, J. R.; Lamprecht, B.; Schider, G.; Ditlbacher, H.; Felidj, N.; Leitner, A.; Aussenegg, F. R. *Opto-Electro. Rev.* **2002**, *10*, 217−224.
(8) Barnes, W. L.; Dereux, A.; Ebbesen, T. W. *Nature* **2003**, *424*, 824−830.
(9) Krenn, J. R.; Weeber, J. C. *Philos. Trans. R. Soc. London Ser. A* **2004**, *362*, 739−756
(10) Raether, H. *Surface-Plasmons On Smooth And Rough Surfaces And On Gratings*; Springer: Berlin, 1988; Vol. 111, pp 1−133.
(11) Krenn, J. R.; Ditlbacher, H.; Schider, G.; Hohenau, A.; Leitner, A.; Aussenegg, F. R. *J. Microsc. (Oxford, U.K.)* **2003**, *209*, 167−172.
(12) Ditlbacher, H.; Krenn, J. R.; Schider, G.; Leitner, A.; Aussenegg, F. R. *Appl. Phys. Lett.* **2002**, *81*, 1762−1764.
(13) Maier, S. A.; Friedman, M. D.; Barclay, P. E.; Painter, O. *Appl. Phys. Lett.* **2005**, *86*, 071103.
(14) Weeber, J. C.; Lacroute, Y.; Dereux, A.; Devaux, E.; Ebbesen, T.; Girard, C.; Gonzalez, M. U.; Baudrion, A. L. *Phys. Rev. B* **2004**, *70*, 235406.
(15) Smolyaninov, II.; Mazzoni, D. L.; Mait, J.; Davis, C. C. *Phys. Rev. B* **1997**, *56*, 1601−1611.
(16) Andersen, P. C.; Rowlen, K. L. *Appl. Spectrosc.* **2002**, *56*, 124A−135A.
(17) Seidel, J.; Grafstrom, S.; Eng, L.; Bischoff, L. *Appl. Phys. Lett.* **2003**, *82*, 1368−1370.
(18) Bouhelier, A.; Huser, T.; Tamaru, H.; Guntherodt, H. J.; Pohl, D. W.; Baida, F. I.; Van Labeke, D. *Phys. Rev. B* **2001**, *63*, 155404.
(19) Xie, Y.; Zakharian, A. R.; Moloney, J. V.; Mansuripur, M. *Opt. Express* **2004**, *12*, 6106−6121.
(20) Bravo-Abad, J.; Martin-Moreno, L.; Garcia-Vidal, F. J. *Phys. Rev. E* **2004**, *69*, 026601.
(21) Lindberg, J.; Lindfors, K.; Setala, T.; Kaivola, M.; Friberg, A. T. *Opt. Express* **2004**, *12*, 623−632.
(22) Salomon, L.; Bassou, G.; Aourag, H.; Dufour, J. P.; de Fornel, F.; Carcenac, F.; Zayats, A. V. *Phys. Rev. B* **2002**, *65*, 125409.
(23) Hubert, C.; Rumyantseva, A.; Lerondel, G.; Grand, J.; Kostcheev, S.; Billot, L.; Vial, A.; Bachelot, R.; Royer, P.; Chang, S. H.; Gray, S. K.; Wiederrecht, G. P.; Schatz, G. C. *Nano Lett.* **2005**, *5*, 615−619.
(24) Vanlabeke, D.; Barchiesi, D. *J. Opt. Soc. Am. A* **1993**, *10*, 2193−2201.
(25) Yin, L.; Vlasko-Vlasov, V. K.; Rydh, A.; Pearson, J.; Welp, U.; Chang, S. H.; Gray, S. K.; Schatz, G. C.; Brown, D. B.; Kimball, C. W. *Appl. Phys. Lett.* **2004**, *85*, 467−469.
(26) Seidel, J.; Baida, F. I.; Bischoff, L.; Guizal, B.; Grafstrom, S.; Van Labeke, D.; Eng, L. M. *Phys. Rev. B* **2004**, *69*, 121405.
(27) Liu, Z.; Wei, Q.-H.; Zhang, X. *Nano Lett.* **2005**, *5*, 957−961.
(28) Ditlbacher, H.; Krenn, J. R.; Hohenau, A.; Leitner, A.; Aussenegg, F. R. *Appl. Phys. Lett.* **2003**, *83*, 3665−3667.

NL051013J